

ACCELERATION OF SOLAR WIND IONS BY NEARBY  
INTERPLANETARY SHOCKS: COMPARISON OF  
MONTE CARLO SIMULATIONS WITH ULYSSES OBSERVATIONS

Matthew G. Baring<sup>1</sup>

Laboratory for High Energy Astrophysics, Code 661,  
NASA Goddard Space Flight Center, Greenbelt, MD 20771, U.S.A.  
*baring@lheavx.gsfc.nasa.gov*

Keith W. Ogilvie

Laboratory for Extraterrestrial Physics, Code 692,  
NASA Goddard Space Flight Center, Greenbelt, MD 20771, U.S.A.  
*u2kwo@lepvax.gsfc.nasa.gov*

Donald C. Ellison

Department of Physics, North Carolina State University,  
Box 8202, Raleigh NC 27695, U.S.A.  
*don\_ellison@ncsu.edu*

and

Robert J. Forsyth

The Blackett Laboratory, Imperial College,  
Prince Consort Road, London SW7 2BZ, U.K.  
*r.forsyth@ic.ac.uk*

---

<sup>1</sup>Compton Fellow, Universities Space Research Association

## ABSTRACT

Various theoretical techniques have been devised to determine distribution functions of particles accelerated by the first-order Fermi mechanism at collisionless astrophysical shocks. The most stringent test of these models as descriptors of the phenomenon of diffusive acceleration is a comparison of the theoretical predictions with observational data on particle populations. Such comparisons have yielded good agreement between observations at the quasi-parallel portion of the Earth’s bow shock and three theoretical approaches, namely Monte Carlo kinetic simulations, hybrid plasma simulations, and numerical solution of the diffusion-convection equation. Testing of the Monte Carlo method is extended in this paper to the realm of oblique interplanetary shocks: here observations of proton and  $He^{2+}$  distributions made by the SWICS ion mass spectrometer on Ulysses at nearby interplanetary shocks (less than about 3AU distant from the sun) are compared with test particle Monte Carlo simulation predictions of accelerated populations. The plasma parameters used in the simulation are obtained from measurements of solar wind particles and the magnetic field upstream of individual shocks; pick-up ions are omitted from the simulations, since they appear, for the most part, at greater heliospheric distances. Good agreement between downstream spectral measurements and the simulation predictions are obtained for two shocks by allowing the parameter  $\lambda/r_g$ , the ratio of the mean-free scattering length to the ionic gyroradius, to vary in an optimization of the fit to the data; generally  $\lambda/r_g \lesssim 5$ , corresponding to the case of strong scattering. Simultaneous  $H^+$  and  $He^{2+}$  data, presented only for the April 7, 1991 shock event, indicate that the acceleration process is roughly independent of the mass or charge of the species. This naturally arises if all particles interact elastically with a massive background, as occurs in collisionless “scattering” off a background magnetic field, and is a patent property of the Monte Carlo technique since it assumes elastic and quasi-isotropic scattering of particles in the local plasma frame.

*Subject headings:* Cosmic rays: general — particle acceleration — shock waves — diffusion

## 1. INTRODUCTION

Particle acceleration at collisionless shocks is believed to be a common phenomenon in space plasmas belonging to a diversity of environments, ranging from the inner heliosphere to the central regions of distant galaxies (e.g. Blandford and Eichler 1987). Evidence to support the belief that such a mechanism can efficiently produce non-thermal particles includes direct measurements of accelerated populations in various energy ranges at the Earth’s bow shock (e.g. Scholer et al. 1980; Ipavich, Scholer and Gloeckler 1981; Möbius et al. 1987; Gosling et al. 1989) and interplanetary shocks (for the pre-Ulysses era see, for example, Sarris and Van Allen 1974; Gosling et al. 1981; Decker, Pesses and Krimigis, 1981; Kennel et al. 1984; Tan et al. 1988), and indirect evidence provided by the observation of non-thermal electromagnetic radiation in distant cosmic sources such as supernova remnants and exotic galaxies and the very existence of cosmic rays. The motivations for developing theories of shock acceleration are therefore obvious, and several popular approaches have emerged over the last twenty years. One of these is the Monte Carlo technique of Ellison and Jones (e.g. see Jones and Ellison, 1991, and references therein) which nicely describes the injection and acceleration of particles from thermal energies, at the same time minimizing the complexities of the underlying microphysics while retaining the essential ingredients of the Fermi acceleration mechanism.

While theoretical work can provide considerable understanding of the diffusive shock acceleration process, the test of its appropriateness to physical environments can only be made by comparison of model predictions with observational data. This has been done very successfully (Ellison, Möbius and Paschmann 1990; see also Ellison and Möbius 1987) in the case of the quasi-parallel portion of the Earth’s bow shock, comparing spectral predictions of the aforementioned Monte Carlo simulation with proton,  $\text{He}^{2+}$  and C, N and O ion particle distributions obtained by the AMPTE experiment. Using the solar wind temperatures of the different ionic species as input for the simulation upstream of the bow shock, downstream particle distributions were obtained from the simulation and compared with the AMPTE data: the agreement was impressive. An important conclusion of this comparison was that the data implied that the dynamic effects of the accelerated particles are crucial to the determination of the shock structure. This feature is a consequence of the quasi-parallel bow shock being a fairly strong shock (i.e., Mach number about 7) and a comparatively efficient accelerator ( $\gtrsim 15\%$  of the solar wind energy flux goes into superthermal particles; see Ellison, Möbius and Paschmann 1990). Since this pioneering work, successful comparisons of other theoretical techniques with data from the Earth’s bow shock have been performed. These include the hybrid plasma simulations of Trattner and Scholer (1991, 1993) and of Giacalone and coworkers (described in Giacalone, Burgess, Schwartz and Ellison 1992, 1993), which yielded quite reasonable agreement with both the bow shock data and the Monte Carlo technique (Ellison et al. 1993). Very recently, Kang and Jones (1995) have obtained solutions to the convection-diffusion equation for particle acceleration at parallel shocks that generate particle distributions similar to the bow shock observations and both the Monte Carlo and hybrid simulations.

It is natural to extend such comparisons to other shock environments. The Ulysses spacecraft has provided the opportunity for an application of this work to interplanetary (IP) shocks, and the high quality and comparative abundance of the spectral data (e.g. see Ogilvie, et al. 1993; Gloeckler, et al. 1995; Baring et al. 1995) obtained by the SWICS instrument aboard Ulysses enhances the significance of such tests of theoretical models. This paper presents results from our program of fitting the Ulysses observations at oblique interplanetary shocks with Monte Carlo simulation output. This has become possible following the generalization of the Monte Carlo technique to treat oblique shocks (Baring, Ellison and Jones 1993, 1994) and to examine cases of strong scattering turbulence (Baring, Ellison and Jones 1995; Ellison, Baring and Jones 1995). Shorter presentations of these comparisons between theory and experiment are enunciated in Baring et al. (1995) and Baring, Ogilvie and Ellison (1995). In this paper, our simulations are confined to test particle implementations for simplicity, which is quite appropriate for the weak IP shocks considered here (discussed in Section 4.2). Note that this is not the first attempt to fit interplanetary shock data with Monte Carlo simulation results: Ellison and Eichler (1984) fit International Sun-Earth Explorer (ISEE) 3 proton data (taken from Gosling et al. 1981) of the IP shock detected on 27th August 1978 with considerable success (see also Ellison 1983 for simultaneous  $He^{2+}$  data fits). However, their simulations were restricted to the case of truly parallel shocks, while the observed shock was only quasi-parallel. Therefore, having simulations of oblique shocks now at our disposal, we are in a position to model IP shocks more realistically than Ellison and Eichler (1984) and assess how the strength of particle scattering influences the acceleration process. We note also that Jones and Kang (1995) and Kang and Jones (1996) have very recently applied their convection-diffusion equation technique to the IP shock  $H^+$  data presented in Baring et al. (1995), again with considerable success in their theory/observation comparison.

In this paper we compare the SWICS measurements of proton and  $He^{2+}$  distributions downstream of interplanetary shocks observed at 2.7–3.2AU from the sun with the simulation output, using upstream measurements of the solar wind quantities to determine the shock parameters for the model. Using a single free parameter  $\lambda/r_g$ , the ratio of the mean-free path for scattering to the ionic gyroradius, to describe the strength of the scattering turbulence, excellent fits of the theory to the observations are obtained for two of our chosen shocks when strong scattering is present, i.e. when  $\lambda/r_g \lesssim 10$ . We regard this as significant confirmatory evidence for the existence of strong turbulence in IP shocks, a result that is borne out in magnetic field data (e.g. Tsurutani, Smith and Jones 1983 for ISEE 3 observations; Viñas, Goldstein and Acuña 1984 for Voyager spacecraft measurements; Balogh et al. 1993 and Section 5.2 here for Ulysses magnetometer results). Furthermore, the simultaneous observations of  $H^+$  and  $He^{2+}$  spectra are remarkably similar (except for normalization) when plotted on a velocity scale, indicating that the acceleration process treats particles of a given speed almost identically despite differences in mass or charge. Such a situation is expected if all particles interact elastically with a massive background; the Monte Carlo technique naturally reproduces this definitive property as a consequence of its assumption of elastic scattering of particles in the local plasma frame. Our attention is confined here to shocks less than 3.5AU distant from the sun, encountered by Ulysses in the first half of 1991. Few pick-up ions, in

particular protons, are evident at heliospheric distances less than around 3.2AU. Interstellar pick-up ions, which can participate in the acceleration process, are not incorporated in the simulation results presented here. The reader is referred to Gloeckler et al. (1994, 1995) for interesting Ulysses observations of IP shocks with strong signals from pick-up hydrogen,  $He^+$  and  $He^{2+}$ . Before detailing our fitting procedure and results in Section 4, we describe briefly the SWICS instrument in Section 2 and the Monte Carlo simulation (see Section 3). The paper concludes with a discussion of the differences between our IP shocks and the quasi-perpendicular portions of the Earth’s bow shock, possible signatures of pick-up protons in one of our candidate shocks, and concurrent Ulysses magnetometer data.

## 2. THE SWICS SPECTROMETER ON ULYSSES

The Solar Wind Ion Composition Spectrometer (SWICS) on the Ulysses spacecraft measures the intensity and distribution functions of solar wind and suprathermal ions over a range of energy per charge from 0.6 to 60 keV/e in 64 logarithmically spaced steps with energy resolution  $\Delta E/E \sim 0.04$ . The energy-per-charge analysis is combined with post-acceleration through a potential difference of 23 kV, and followed by time-of-flight and energy measurement to identify ionic mass and charge states. Because of the double and triple coincidences used, the background levels are very low, typically less than one count per hundred hours. This permits measurements of very low flux levels. The instrument uses a curved multi-slit collimator, which covers  $57^\circ \times 4^\circ$  in angle, fixed to the spacecraft with the spacecraft spin axis passing through one end. Thus the instrument sweeps out a cone of half-angle  $57^\circ$  as it rotates. The cone is centered approximately in the solar wind direction, and is sampled once per spacecraft revolution, which is 12 seconds in duration. The entire velocity range of observed ionic distribution functions is covered sequentially in 64 of these samples, i.e. once every 13 minutes; hence any variability in the ion populations is undetectable on shorter timescales. In order to restrict the counting rate of the “start” channel plate in the time-of-flight system, the SWICS data processing unit has a mode where the voltage sweep applied to the electrostatic analyser is reversed if the counting rate exceeds a preset number. Since the voltage sweep tracks particles from high to low energy, this safety feature (Gliem et al. 1988) prohibits measurement of the ion distributions much below the channel with peak count rate. This mode was in use early in the Ulysses mission, indeed for the data presented here, but its use was subsequently abandoned, having been deemed unnecessary for instrumental security.

Data used in this manner implicitly assumes that the detected ions are samples of a distribution that is isotropic within this cone, an expedient approximation that is extremely difficult to relax. Careful consideration of particle anisotropies is therefore essential to more refined analysis of the experimental data. For example, the solar wind beam is always completely sampled by a small portion of the collimator, whereas ions accelerated to well above 1000 km/sec are quasi-isotropic and therefore occupy a larger solid angle than does the rotating collimator. Between these cases are suprathermal ions, whose inferred distribution depends somewhat on the precise degree of

anisotropy in the plasma, an unmeasured and therefore assumption-dependent quantity. While such intricacies of data analysis do not affect the qualitative nature of the scientific conclusions presented (this matter will be briefly addressed in Section 4.2), it must be noted that it is the suprathermal (or injected) ions, which have the largest uncertainties due to unknown anisotropies, that are the most influential in the shock acceleration process. For more complete details of the SWICS instrument, see Gloeckler et al. (1992). This study uses measurements of protons and doubly-charged helium only; data on  $He^+$  pick-up ions observed at greater heliospheric distances is presented in Gloeckler et al. (1994). Also, note that data at energies higher than 60 keV have been obtained by the HI-SCALE experiment on Ulysses (described in Lanzarotti et al. 1992). Use of such data was not possible at this stage, and is deferred to future work.

### 3. MONTE CARLO SIMULATIONS OF SHOCK ACCELERATION

The simulation technique (described in detail in Ellison, Jones and Eichler 1981; Jones and Ellison 1991; Baring, Ellison and Jones 1993; Ellison, Baring, and Jones 1996) is a kinematic model, closely following Bell’s (1978) approach to diffusive acceleration; it essentially solves a Boltzmann equation for particle transport involving a collision operator. Particles are injected upstream and allowed to convect into the shock (i.e. mimicking the solar wind), colliding with postulated scattering centers (presumably magnetic irregularities) along the way. As they diffuse between the upstream and downstream regions, they continually gain energy (for a simulation example, see Fig. 3 of Baring, Ellison and Jones 1994), sampling the velocity differential across the shock; this is the principle of the Fermi acceleration mechanism. An important property of the model is that it treats thermal particles like accelerated ones, making no distinction between them. Hence, as the accelerated particles start off as thermal ones, this technique automatically injects particles from the thermal population into the acceleration process, thus circumventing the injection problem that plagues some models of shock acceleration. One valuable consequence of this unified treatment for thermal and non-thermal particles is that modification of the shock hydrodynamics by the accelerated population can easily be incorporated to forge a fully self-consistent model of acceleration and shock structure. Such non-linear hydrodynamics were included in the modelling of the quasi-parallel portion of the Earth’s bow shock (Ellison, Möbius and Paschmann 1990), but is not important for the interplanetary shocks examined in this paper: this is evident from the spectral data presented in Section 4.2 below. Shock modification is therefore not included in the present modelling. However, we note that it may prove necessary to include such non-linear effects when performing fits over a much broader range of energies than is the case here, for example when including HI-SCALE data.

The scattering is assumed to be elastic and to isotropize particle momenta in the local fluid frame, i.e. to mimic large-angle collisions with field turbulence that is anchored in this frame. Such collisions might well be expected in view of the quite turbulent fields observed in heliospheric shock environments (e.g. Hoppe et al. 1981; Tsurutani, Smith and Jones 1983; Balogh et al. 1993). In

the simulation, particles are allowed to travel between scatterings for a time that is exponentially distributed about the time  $t_c = \lambda/v$ , where  $v$  is the particle speed in the fluid frame and  $\lambda$  is the scattering mean free path in the fluid frame, which is taken to be a power-law function of momentum  $p$ :

$$\lambda = \lambda_0 \left( \frac{r_g}{r_{g1}} \right)^\alpha \propto p^\alpha \quad . \quad (1)$$

Here  $r_g = pc/(QeB)$  is the gyroradius of a particle with momentum  $p$ , charge  $Qe$ , in a magnetic field of strength  $B$  ( $c$  is the speed of light and  $e$  is the electronic charge), and  $r_{g1} = m_p u_{1x}/(eB_1)$  is the gyroradius of a proton with the far upstream speed  $u_{1x}$  (i.e. the component of the upstream flow velocity normal to the shock plane in the rest frame of the shock) in the upstream magnetic field,  $B_1$ . Hereafter,  $x$  denotes distance measured along the shock normal, and subscripts 1(2) will indicate upstream (downstream). Here  $\lambda_0$  is set proportional to the gyroradius  $r_{g1} = mu_{1x}/(eB_1)$  of (low energy) protons of speed  $u_{1x}$ : the ratio  $\lambda_0/r_{g1}$  is an input parameter that is of crucial importance to this study. For simplicity,  $\lambda_0/r_{g1}$  is taken to be the same both upstream and downstream of the shock, a subjective choice that is largely immaterial to the nature of the results presented below.

This simple prescription is perhaps surprisingly appropriate to shocked plasma environments. Bow shock observations (Ellison, Möbius, and Paschmann 1990) indicate that  $1/2 < \alpha < 3/2$ , while  $1/2 < \alpha < 4/5$  can be deduced from ions accelerated in solar particle events (Mason, Gloeckler and Hovestadt 1983), and  $\alpha \sim 1/2$  is obtained from turbulence in the interplanetary magnetic field (Moussas et al. 1992). Plasma simulations (Giacalone, Burgess, and Schwartz 1992) suggest a mean free path obeying Eq. (1) with  $\alpha \sim 2/3$ . Clearly a variety of microphysics can be incorporated in specifying  $\lambda$  and both pitch-angle diffusion (small-angle scattering) and large-angle scattering can be modelled by the simulation. Therefore the attractiveness of this approach is that the overall nature of the diffusive acceleration process can be modelled without the burden of CPU intensive computations of the underlying physical plasma mechanisms. All results presented here are for  $\alpha = 1$ , a choice that nicely guarantees that the ratio  $\lambda/r_g$  is independent of the particle momentum.

The assumption of elasticity of scattering in the local fluid frame is expected to be accurate except perhaps at shocks with very low Alfvénic Mach numbers, where the flow speed does not far exceed the Alfvén velocity and the scattering centers (i.e. Alfvén waves) move in the fluid frame with significant speeds. In the shocks studied here, as is typically the case for interplanetary shock systems, the magnetic field is dynamically important, with Alfvénic Mach numbers in the range of 2.4–4, so that to some degree the elastic scattering assumption is violated. Nevertheless, for the shock parameters relevant to this study, the contribution to particle acceleration resulting from motion of the scattering centers in the local fluid frame is expected to be overshadowed by the first-order acceleration process that is modelled in this paper, and which principally determines the overall shape of model particle distributions. We expect that the major properties of the acceleration mechanism are therefore well-described by elasticity of scattering, and that the deviations from this in IP shock environments will incur only effects of secondary importance. Hence, in the spirit of

this incipient comparison of theory and experiment, we adopt the elastic scattering approximation, and defer examination of the higher order effects that are associated with its violation to future work.

In applications of the Monte Carlo simulation to oblique shocks, particle transport is followed in the de Hoffmann-Teller (HT) frame (de Hoffmann and Teller 1950), where the drift electric field  $\mathbf{E} = (\mathbf{u}/c) \times \mathbf{B}$  is transformed to zero, and the fluid flow is everywhere parallel to the magnetic field. This approach guarantees that shock drift acceleration is automatically included. Also, since our technique does not require detailed computation of the turbulent field structure, it is much faster than hybrid or full plasma codes, and thereby achieves much larger dynamic ranges of momenta for particle distributions than is possible for the plasma simulations. This renders the Monte Carlo approach ideal for spectral comparisons with observational data. There are two variations of the simulation that are employed here: (i) one in which a guiding-center approximation is made (Baring, Ellison and Jones 1994), where the details of the particles' gyromotions are ignored and they conserve their adiabatic moment  $p^2(1 - \mu^2)/2B$  (the so-called *adiabatic approximation*) when interacting with the shock; and (ii) where the exact gyrohelix particle trajectories (e.g. see Ellison, Baring and Jones 1995, 1996) are computed without imposition of the adiabatic approximation in particle-shock interactions. Results from both variations are employed in this paper. Another simplification made in the simulation is the use of a single parameter  $\lambda_0/r_{g1}$  to describe the strength of the scattering turbulence (i.e. cross-field diffusion; see Baring, Ellison and Jones, 1995 for details). This parameter plays a crucial role in determining the efficiency of injection of particles into the non-thermal tail, as is discussed in Section 4.

Our model is implemented in this paper as a test particle simulation, where the accelerated particles make only a small contribution to the dynamics of the fluid flow. This is appropriate for modelling interplanetary shocks, which are of low sonic Mach number and therefore comparatively inefficient at accelerating particles (as discussed in Section 4.2). For a full discussion of the non-linear effects associated with high Mach number shocks, see Ellison, Baring, and Jones (1996). The usual hydrodynamic quantities of the downstream fluid are therefore simply determined from those in the upstream region by the full MHD Rankine-Hugoniot relations (e.g. Decker 1988). In the IP shock applications here the magnetic field is high enough to be dynamically important. Hence, all characteristics of the shocks depend only on the shock compression ratio  $r = u_{1x}/u_{2x}$ , the sonic Mach number  $\mathcal{M}_s \approx [m_p u_{1x}^2 / (\gamma k T_1)]^{1/2}$ , where  $T_1 = T_{p1} + T_{e1}$  is the total upstream temperature,  $\gamma = 5/3$  is the adiabatic index, and the Alfvénic Mach number  $\mathcal{M}_A \approx [4\pi n_p m_p u_{1x}^2 / B^2]^{1/2}$ . Simulation output principally includes particle distributions in any desired frame of reference at any position upstream or downstream of the shock.

#### 4. COMPARISON OF MONTE CARLO SPECTRA WITH SWICS DATA

Before comparing in detail the Monte Carlo particle distributions with the SWICS measurements downstream of our three case-study IP shocks, it is appropriate first to indicate what input

parameters for the simulations were derived from various pieces of observational data. The three shocks chosen were observed early in the Ulysses mission, specifically on day 97 of 1991 (April 7; denoted 91097), day 118 of 1991 (April 28; denoted 91118), and day 147 of 1991 (May 27; denoted 91147), when Ulysses was in the ecliptic before its encounter with Jupiter. Motivation for our choices included availability of high quality spectra (i.e. with good statistics) in these shocks, and *relatively* simple shock structure and spectra during this phase of the mission. These shocks appear to be representative of the shocks encountered by Ulysses in the first half of 1991. The prominence of accelerated particles in the environs of many shocks other than those studied here suggests that the basic physical conclusions drawn in this paper can be extended to a host of other IP shocks detected during this early phase of the Ulysses mission.

Of the three shocks in our case study, two (91097 and 91118) are freely propagating (travelling) interplanetary shocks and the other (91147) is a member of a co-rotating shock pair. *Co-rotating interaction regions* (CIRs e.g. see Hundhausen 1973 for a description), frequently observed by Ulysses (e.g. Gosling et al. 1993, 1995), result from the evolution of regions where solar wind regions of higher speed impinge upon lower speed wind that emanates from the equatorial region of the sun. At the heliocentric distances considered here, the collision results in a forward and reverse shock pair on either side of an interface; the shocks propagate away from the interface, which itself moves away from the sun at a speed greater than that of the solar wind. We have selected the forward shock on day 91147 only for our study.

#### 4.1. Observational Parameters and Simulation Input

Following the approach that Ellison, Möbius and Paschmann (1990) used when comparing Monte Carlo spectra with observations at the quasi-parallel portion of the Earth’s bow shock, we use here measurements of various solar wind quantities upstream of three interplanetary shocks to set the input parameters for the Monte Carlo simulation runs. The simulation then makes predictions of downstream spectra, which are then compared with SWICS data downstream of these IP shocks to ascertain whether consistency between experiment and theory can be achieved.

The various input quantities used in the Monte Carlo runs are tabulated in Table 1 for the three selected IP shocks, together with their corresponding heliocentric distances. All the quantities in the upper zone except for the shock velocities  $u_s$  were directly determined from measurements by various instruments on Ulysses;  $u_s$ , the ion temperatures and the shock Mach numbers are inferred from the measured quantities. Specifically,  $u_s$  for shocks 91097 and 91147 are taken from the published listing of Burton et. al. (1992), which cites a shock speed of 2 km/sec for 91118. This erroneous result, probably typographical, can be corrected by inferring the value of  $u_s$  based on the other measurable quantities and the total Mach number of 1.97 cited by Burton et. al. (1992) and Balogh et al. (1992). The result is an estimate of 165 km/sec, which implicitly has at least a 10% uncertainty since the Mach number can be no more accurate than the least certain measurable, which is the field obliquity  $\Theta_{B1}$ . Unpublished data on plasma speeds combined with

the measured obliquity were used to verify the consistency of this estimate.

The values listed in Table 1 for the thermal velocities  $v_{th}$  were taken from Gaussian fits to spectral data less than an hour upstream of the respective shocks. The peak of the phase space distribution was fit with a form proportional to  $\exp[-v^2/v_{th}^2]$ . Upstream densities  $n_{H^+}$  and  $n_{He^{2+}}$  are quoted for similar timescales. The upstream magnetic field values  $B_1$  are averages on timescales of about a minute, and their accuracy is limited by temporal/spatial fluctuations, which are discussed in Section 5. As a consistency check on the tabulated values, we used the Monte Carlo code to generate solutions of the Rankine-Hugoniot relations for the field compression ratio  $B_2/B_1$  from the input solar wind quantities, and these agreed to within about 8% of the ratios published by experimental teams (Balogh et al. 1995, Hoang et al. 1995). The solar wind electron temperatures for the 91097 and 91147 shocks are published in Hoang et al. (1995), where they indicate large uncertainties ( $\sim 30\%$ ). No such listing for the 91118 event was available, so we used the best fit radial dependence temperature at 2.85 AU obtained from Phillips et al. (1995), representing a length scale of the order of 0.25AU. This choice is subject to large uncertainty since the electron temperature varies on short timescales. With the exception of the shock obliquity, uncertainties for the measured solar wind quantities largely reflect limits set by fluctuations in these quantities and the choice of temporal binning. Determination of  $\Theta_{B1}$  is intrinsically problematic because it is difficult to establish the plane of the shock in a turbulent environment with measurements made only along the spacecraft trajectory.

Clearly the uncertainties in most shock parameters are of the order of 10%, which must be taken into account in the following theory-data comparison. Uncertainties are not quoted in Table 1 for the derived quantities, i.e. ion temperatures and Mach numbers. As indicated, the values of  $\mathcal{M}_T$  listed in Table 1 for 91097 and 91147 are derived using the measured values in the upper zone, whereas the value of 2.07 for the 91118 shock was used to estimate the shock velocity. Simple formulae for the sonic and Alfvénic Mach numbers that are scaled to suit typical IP shock parameters can be quickly written down:

$$\mathcal{M}_S \approx 8.52 \frac{u_{100}}{\sqrt{T_{p4} + T_{e4}}} \quad , \quad \mathcal{M}_A \approx 4.58 \frac{u_{100}}{B_{-5}} \sqrt{n_{H^+}} \quad , \quad (2)$$

where  $u_{100}$  is the shock speed  $u_s$  in units of 100 km/sec,  $T_{p4}$  and  $T_{e4}$  are the proton and electron temperatures in units of  $10^4$  K,  $B_{-5}$  is the upstream field strength in units of  $10^{-5}$  Gauss, and  $n_{H^+}$  is the proton density in  $\text{cm}^{-3}$ , which is approximately equal to the electron density  $n_e$  (an 8% difference arises due to the alpha particle abundance in the solar wind). The comparable values of these two Mach numbers for the IP shocks studied here indicate that the fields are dynamically important; their proximity to unity suggests that the shocks are weak and therefore are relatively inefficient particle accelerators (e.g. compared to the Earth’s bow shock), a feature that is borne out in their spectral data. Note that we neglected to explicitly include the effects of  $He^{2+}$  on the dynamics of the 91097 event. While alpha particles comprise about 4% of the solar wind population, and therefore are about 16% abundant by mass, they also comprise roughly the same percentage of the thermal energy (i.e. 16% ; a coincidence specific to 91097). Hence, dynamically they contribute

about the same fraction of the ram pressure (i.e. the numerator of  $\mathcal{M}_s^2$ ) and the thermal pressure (denominator) and hence have marginal influence on the value of  $\mathcal{M}_s$ . Helium data are considered only for the April 7, 1991 shock since they were of almost comparable quality to the proton data; the non-thermal tails of the He spectra for the 91118 and 91147 events had insufficient statistical quality for the purposes of this analysis.

## 4.2. The Spectral Comparison

The comparisons of the Monte Carlo model results with the IP shock data are performed in the spacecraft frame, using boost speeds between the shock and spacecraft frames in the range of around 360–430 km/sec, depending on the shock. Such speeds were deduced from the speeds associated with the thermal peaks upstream and downstream of each of the shocks, and were consistent with estimates (subject to large uncertainties) determined from the shock parameters listed in Burton et al. (1992). A multiplicative factor is applied to the Monte Carlo upstream proton distributions to render them commensurate with the solar wind density. The fitting of the observed spectral data with the simulation output is then essentially achieved by adjusting a *single* free model parameter  $\lambda_0/r_{g1}$  by visual inspection. This parameter, whose physical significance is discussed shortly, is a scaling parameter for the simulation, being the ratio of the mean free path to the gyroradius of particles with speed  $u_{1x}$  (see Section 3). The scientific conclusions of this paper are amply defined via this simple visual procedure.

Figure 1 depicts the data/theory comparison for the IP shock on April 28, 1991 (day 91118) using the guiding center (GC) version of the simulation. The experimental data are taken over a period of a few hours on the downstream side of the shock where the distribution was relatively steady in time; throughout this paper the uncertainties on the data points denote one standard deviation. A similar comparison is made in Fig. 2 using the gyrohelix (GH) version of the code. The two fits are quite similar with the gyrohelix version requiring a somewhat lower value of  $\lambda_0/r_{g1}$  to approximate the data. Note that this period of data collection is chosen to be quite long in order to achieve good statistics. The base instrumental spectral time resolution of 13 minutes corresponds to the order of 400 gyroperiods  $T_g$  for protons behind the shock (where  $B \sim 5 \times 10^{-5}$  Gauss), where  $T_g \equiv \omega_c^{-1} = m_p c / (eB) \approx 10.4/B_{-5}$  sec. Here  $\omega_c$  is the gyrofrequency and  $B_{-5}$  is the field in units of  $10^{-5}$  Gauss. Hence the much longer integration times used in the spectral comparisons of this Section generally represent several thousand gyroperiods. The properties of the shock itself are deduced from the much more frequent measurements of the magnetic field.

The SWICS particle distribution data used here and throughout this paper are phase space densities  $f(v)$ , for which  $v^2 f(v) dv$  represents a particle density; these are essentially the count rate (i.e. detected flux) divided by velocity to the fourth power. As the velocities are in units of km/sec, the distribution functions depicted here integrate over velocity to yield densities in units of particles per cubic kilometre. Since data are taken in the spacecraft frame, the thermal peak exhibits a large positive offset of a few hundred km/sec relative to the frame of the shock,

reflecting the solar wind speed in the ecliptic. The counts are dead-time corrected, but do not include complete corrections for instrumental geometry and response. Such corrections are not yet fully implemented, but are expected to produce at most about a factor of a 2–3 difference to the distribution. Thus these corrections are small over the dynamic range of seven orders of magnitude for the distributions in the figures of this section, and it is evident that their inclusion would not significantly alter the physical conclusions deduced from the comparisons presented.

Figures 1 and 2 can be used to estimate the contribution of the accelerated population to the dynamics of the 91118 shock. The phase space densities  $f(v)$  used here can be multiplied by a factor of  $v^4$  to yield energy density distributions. This weighting should be considered in the shock rest frame, where treatment of the dynamics is simplest. In this frame, for the IP shocks considered here, the downstream thermal particles typically have speeds around 150 km/sec (i.e. the shock speeds listed in Table 1). Hence in transforming data from the spacecraft to the shock rest frames, clearly a ratio of around 10 in speeds is encompassed in the shock frame by the distributions in Figs. 1 and 2. It follows that the high speed particles have at most a few percent of the energy density contained in the thermal population, a result that extends to the other two shocks. The accelerated populations detected by the SWICS instrument are therefore dynamically unimportant, thereby justifying the test particle implementation in this paper.

The agreement between experiment and theory in Figs. 1 and 2 is impressive, with only small differences in the downstream temperature (for the guiding center implementation of the code) and shape of the suprathermal portion of the distributions being apparent. The fits are of comparable quality for the two types of particle convection employed, namely (i) exact gyrohelix determination and (ii) use of the guiding center approximation with the added assumption of adiabatic moment conservation. Furthermore, the data strongly constrains the possible values of  $\lambda_0/r_{g1}$  (typically  $\pm 0.1$ ). While these two versions of the simulation produce somewhat different estimates of the parameter  $\lambda_0/r_{g1}$  due to their differing prescriptions for the way particles cross the shock, the physical conclusions drawn from these values are similar. It appears that exact gyrohelix computations are slightly less efficient at injecting particles from the thermal population in highly oblique shocks. The physical importance of this parameter follows from its crucial role in determining the extent of cross-field diffusion. If  $\kappa_{\parallel}$  and  $\kappa_{\perp}$  are the diffusion coefficients respectively parallel and perpendicular to the average magnetic field, then the two can be related using the standard kinetic theory result (e.g. Axford 1965; Forman, Jokipii and Owens 1974) for a mean free path  $\lambda$  and particle gyroradius  $r_g$  in the local fluid frame:

$$\kappa_{\perp} = \frac{\kappa_{\parallel}}{1 + (\lambda/r_g)^2} . \quad (3)$$

Non-zero values of  $\kappa_{\perp}$  (i.e. non-infinite  $\lambda/r_g$ ) amount to the presence of cross-field diffusion. This identity is tantamount to shifting a particle by approximately one gyroradius in *any direction* during scatterings with the turbulent magnetic field. Jokipii (1987) observed that there is no general consensus as to the form of this relationship, so that the choice of the ratio is somewhat subjective, being restricted only by the requirement that a particle move of the order of a gyroradius in a

scattering. Clearly then, large values of  $\lambda/r_g$  ( $\equiv \lambda_0/r_{g1}$  in this application) represent weak cross-field diffusion, where the field lines are almost laminar, while small values ( $\lambda/r_g \ll 1$ ) define the regime of Bohm (isotropic) diffusion, which may be attained in strongly turbulent fields.

Using an analysis of particle acceleration times, Ellison, Baring and Jones (1995) demonstrated that the Monte Carlo technique accurately simulates the kinetic theory result in equation 3. Besides confirming Jokipii’s (1987) observation that shocks of higher obliquity are *faster* accelerators, the analysis of Ellison, Baring and Jones (1995) indicated that the efficiency of injecting particles into the Fermi acceleration mechanism is a strongly *decreasing* function of shock obliquity and the strength of the scattering parameter  $\lambda_0/r_{g1}$  (see also Baring, Ellison and Jones 1993). This sensitivity is a crucial feature of the acceleration process that compels the range of  $\lambda_0/r_{g1}$  in the fit to be narrow. The origin of this dependence can be simply understood. In the de-Hoffmann Teller frame, the diffusion length scale of low energy (i.e. thermal) particles along the field is roughly given by  $\lambda_0$ , while their diffusion length normal to the field is represented by the gyroradius  $r_{g1}$ . In oblique shocks, specifically those with  $\Theta_{Bn1} \gtrsim 30^\circ$ , convective return of thermal ions to the shock from the downstream side is inhibited so that the injection into the Fermi acceleration mechanism is suppressed (Baring, Ellison and Jones 1993, 1994). From simple considerations of geometry, this is clearly circumvented by cross-field diffusion when  $r_{g1}/\lambda_0 \gtrsim \cot \Theta_{Bn2}$  (for  $\Theta_{Bn2}$  being the downstream field obliquity) and particle return to the shock is enabled (Baring, Ellison and Jones 1993; Ellison, Baring and Jones 1995). Hence it is expected that the efficiency of injection and acceleration will scale inversely with the parameter  $(\lambda_0/r_{g1})/(1 + \tan \Theta_{Bn2})$ .

Clearly then, when  $\lambda_0/r_{g1} \gg 1$  and cross-field diffusion is small, the accelerated population is strongly suppressed in highly oblique shocks, contrary to the observational data. The light solid histogram in Fig. 1 is the predicted simulation in the limit of  $\lambda_0/r_{g1} \rightarrow \infty$ , starkly illustrating the lack of acceleration from thermal energies. Therefore in the fits in Figs. 1 and 2, where the high velocity portions of the histograms shift up and down rapidly relative to the thermal peaks with only modest variations in  $\lambda_0/r_{g1}$ , only small values of  $\lambda_0/r_{g1}$  are allowed. It can be simply deduced that, within the context of this Monte Carlo model, the significant acceleration efficiency implies that strong scattering is operating in this traveling interplanetary shock. A similar conclusion is reached in the subsequent presentation for other IP shocks, which are also efficient accelerators, and is suggestive of turbulent magnetic fields in interplanetary shock environments. Since the efficiency is extremely sensitive to the shock obliquity, the most uncertain of the observables, improved measurements will refine estimates of  $\lambda_0/r_{g1}$ , but will not alter the implication of strong scattering acting in interplanetary shocks. Note that hereafter,  $\lambda_0/r_{g1}$  and  $\lambda/r_g$  will be used interchangeably due to their identity, which is the result of assuming  $\alpha = 1$  in the scattering formula in equation (1).

Figure 3 displays the spectral comparison for the IP shock on April 7, 1991 (day 91097) using the guiding center (GC) version of the simulation. The SWICS data are again taken over a period of a few hours (i.e. thousands of gyroperiods) on the downstream side of the shock, but this time, the data permitted presentation of the  $He^{2+}$  phase space distribution also. The relative normalizations of the upstream distributions for protons and  $He^{2+}$  were deduced from the abundance ratio implied

by Table 1, and are not free parameters in the model. The fit is clearly impressive for the proton spectrum, and is equally encouraging for the alpha particles considering that just *one* parameter ( $\lambda/r_g$ ) is used to reproduce both the spectral shape *and* the relative populations of both accelerated ion species. Again, the relatively low value of  $\lambda/r_g = 3.7$  implies strong scattering.

At first sight, it seems remarkable that just one choice of  $\lambda/r_g$  can fit the the two species so nicely. However, this is consistent with the observed spectra being essentially independent of mass and charge, i.e. depending only on velocity kinematics. Since the inferred upstream  $He^{2+}$  temperature is about four times that of the protons, the input for the simulation is roughly independent of mass and charge. If, in addition, all particles interact nearly elastically with a massive background, namely magnetic field turbulence “anchored” in the fluid frame, the acceleration process, and therefore the spectral shape and injection efficiency, will depend only on particle velocities. Since the Monte Carlo simulation makes just this elastic assumption (i.e. in Eq. [1]), it is not surprising that we can accurately model the observations in this test-particle regime. Given such dependence on the kinematics, the relative normalizations of the  $H^+$  and  $He^{2+}$  data downstream are largely determined by their relative abundances upstream. The results in Fig. 3 indicate the high accuracy of such a scattering assumption in traveling interplanetary shocks when interstellar pick-up ions are unimportant.

Another noteworthy feature of this comparison is that this is the first time that the upstream abundance ratio *of thermal ions* has been used to set relative population levels in a theory/data comparison of acceleration at shocks somewhere in the heliosphere. Due to the inability of the 3D-Plasma Instrument on the AMPTE/IRM spacecraft to measure elements heavier than hydrogen, the study of the parallel portion of the Earth’s bow shock by Ellison, Möbius and Paschmann (1990) did not have upstream measurements at thermal energies of elements heavier than hydrogen (downstream observations of non-thermal alpha particles and heavier elements were made above 10 keV/Q by the SULEICA instrument), and so could not determine relative abundances in the local solar wind. It should be noted that the values of  $\lambda/r_g$  obtained in the fits presented here differ somewhat from previous expositions of this data/theory comparison, notably in Baring et al. (1995) and Baring, Ogilvie and Ellison (1995). This difference arises because more refined estimates of the magnetic field and solar wind densities have been used here than in the earlier works, with finite electron temperatures being included, thus revising the input parameters for the shock simulation. The shock strength is somewhat weaker than before, so that estimates for  $\lambda/r_g$  are now lower. We note that recently with the aid of shock parameters from Baring et al. (1995), Kang and Jones (1995) and Kang and Jones (1996) have obtained, comparable fits to the proton data for the 91097 and 91118 shocks using their convection-diffusion equation model of the Fermi acceleration mechanism.

As a contrast to the above data comparisons, it is instructive to study a shock that was encountered at a later stage of Ulysses’ passage away from the sun. Figure 4 displays the comparison for the IP shock on May 27, 1991 (day 91147), again using the guiding center (GC) version of the simulation, and proton data accumulated over several hours. The choice of  $\lambda/r_g$  is solely influenced

by the fit to the high velocity portion (1000–1800 km/sec) of the data, and again suggests strong scattering. However, the value of  $\lambda/r_g$  is somewhat higher in this shock than in the previous two, due to its lower obliquity. The inaccuracy of the comparison in the suprathermal region contrasts strongly with the previous fits, and is probably indicative of the presence of another proton population (i.e. interstellar pick-up ions), as is discussed below, rather than representing the failure of the Fermi acceleration mechanism. The presence of such pick-up ions, with speeds ranging between zero and twice the solar wind speed, may account for the discrepancy, since the simulation deficiency in Fig. 4 is in precisely this velocity range. The present implementation of the Monte Carlo simulation models injection and acceleration of particles drawn only directly from the thermal population, however, it can be easily adapted to describe additional pre-accelerated populations.

To summarize, in two of our three case studies excellent fits have been obtained, though some small discrepancies exist at thermal and suprathermal energies. The slight deficiencies of the simulation predictions relative to the data in Figs. 1–3 (particularly for the guiding center implementations of the simulation) could be due to subtleties in the microphysics that are omitted from the simulation, such as the presence of a cross-shock potential that would modify the acceleration efficiency, or deviations from the scattering law in equation (1). Furthermore, there may be some suprathermal population present at a level smaller than in Fig. 4 that may distort the distributions from the simple simulation predictions. In addition, the omission from the simulation of non-linear modifications of the shock hydrodynamics by the accelerated population (generally small for IP shocks) might lead to a slightly incorrect estimation of the downstream temperature. Such non-linear effects smooth the shock velocity profile upstream (decelerating the flow) and increase the overall compression ratio, thereby modifying the width of the downstream thermal distribution (e.g. Ellison, Baring and Jones 1996). It must be remembered that the fits attempted here are confined to relatively low particle speeds, and may be degraded or modified somewhat by a future consideration of data at higher energies, such as that obtained by HI-SCALE, where the test-particle Fermi acceleration distributions assume well-known (e.g. see Blandford and Eichler 1987; Jones and Ellison 1991) power-laws.

## 5. DISCUSSION

Perhaps the most remarkable aspect of the observations presented here is simply that low Mach number, highly oblique, interplanetary shocks accelerate significant fractions of thermal solar wind protons and alpha particles to non-thermal energies, and do so with comparable efficiencies. The smooth transition from the thermal portion of the distribution to a non-thermal tail seen in Figs. 1–3, and, to a lesser extent, 4, is a distinctive signature of the direct injection and acceleration of thermal particles, given that no such transition is seen less than an hour upstream of these shocks. This close association of thermal and non-thermal ions in the neighbourhood of these quasi-perpendicular IP shocks is decidedly different behavior from that observed at highly oblique portions

of the Earth’s bow shock, and also from plasma simulation results, which show no significant acceleration of thermal ions at all in shocks of high obliquity.

At quasi-perpendicular parts of the bow shock, reflected field-aligned beams are typically seen propagating back from the shock, and these beams have a much lower  $He^{2+}$ /proton ratio than the ambient solar wind (e.g. Ipavich et al. 1988; Fuselier and Thomsen 1992). These beams are believed to originate when particles specularly reflect off the shock (see Thomsen 1985 for a review), with protons reflecting more easily than  $He^{2+}$ . Downstream from the bow shock, the helium remains at much lower relative density compared to the protons (Fuselier and Schmidt 1994), in contrast to what we see here downstream from IP shocks. The radically different behavior of highly oblique regions of the Earth’s bow shock and the IP shocks considered here is probably the result of the very different relative length scales involved. Both travelling IP shocks and those associated with CIRs have radii of curvature that are much larger than that of the earth’s bow shock, at least for large distances from the sun. The diffusion length of suprathermal particles at the bow shock is comparable to the bow shock radius, and reflected or accelerated particles that are produced near the tangent point of the solar wind magnetic field with the shock, where the field has very little turbulence, are quickly swept away and do not have the chance to generate local turbulence. An IP shock, on the other hand, is much larger compared to diffusion length scales so that particles generated at quasi-perpendicular shock environments can remain in the system long enough to maintain much larger levels of turbulence.

An idea of the scale lengths associated with these shock systems can be gained from the gyroradii of the detected particles. At non-relativistic velocities  $v$ , a particle of mass number  $A$  and charge state  $Q$  has a gyroradius of  $r_g = (A/Q) m_p v c / (eB)$ , which can be translated into units of relevance to the plasma environment considered here:

$$r_g(\text{km}) = \frac{A}{Q} \frac{10.43}{B_{-5}} v_{\text{km/sec}} = \frac{A}{Q} \frac{4567}{B_{-5}} \sqrt{E_{\text{keV}}} \quad , \quad (4)$$

where  $B_{-5}$  is the field strength expressed in units of  $10^{-5}$  Gauss, and  $E_{\text{keV}}$  is the particle energy in keV. Clearly, since the IP shock velocities are of the order of 100–300 km/sec, thermal protons have gyroradii around  $10^3$  km, and even the most energetic ions detected by SWICS have gyroradii (and therefore mean free paths) much less than the typically huge IP shock scale ( $> 10^7$  km). This behaviour differs strongly from that at the Earth’s bow shock, which has particles accelerated to comparable energies but a much smaller radius curvature, of the order of  $10^4$  km. An important byproduct of these scale length estimates is that the use of a planar shock model in this study is both expedient and justifiable for interplanetary shock applications. The angle between the shock normal and the magnetic field,  $\Theta_{Bn1}$ , is constant for much longer distances along the faces of such shocks than typical particle mean free paths. As the efficiency of shock acceleration is a strong function of  $\Theta_{Bn1}$  (e.g. Baring, Ellison and Jones 1993; Ellison, Baring and Jones 1995, 1996), interplanetary shocks are very suitable for comparison with theory, since the observations at a given point with given  $\Theta_{Bn1}$  are not contaminated by particles accelerated at locales of the shock where  $\Theta_{Bn1}$  is different.

In regards to full plasma simulations, to our knowledge, all published 1-and 2-dimensional plasma simulation results for shocks with  $\Theta_{Bn1} \gtrsim 60^\circ$  fail to show significant acceleration of thermal ions (e.g. Liewer, Goldstein, and Omid 1993; Liewer, Rath, and Goldstein 1995; Kucharek and Scholer 1995). We believe this to be a consequence of an unphysical suppression of cross-field diffusion in simulations with field geometries of less than three dimensions (Jokipii, Kóta, and Giacalone 1993; Jokipii and Jones 1996). Since cross-field diffusion is essential for allowing downstream particles to recross the shock, as noted above, its suppression will eliminate particle injection and possibly also subsequent self-generation of field turbulence. The kinematic Monte Carlo technique simply incorporates a prescription of such particle diffusion via the parameter  $\lambda/r_g$ , and hence is inherently three-dimensional in its description of particle motions.

### 5.1. Pick-up Ions?

The excellence of the data fits to the 91097 and 91118 shocks, and the comparatively poor fit to the 91147 data, could be considered consistent results if an extra population of seed particles for the acceleration mechanism were present in the 91147 event, thereby circumventing the deficiency seen in Fig. 4. Interstellar pick-up ions, which are neutral when they enter the heliosphere, are ionized by the solar UV flux or by charge exchange with the solar wind (e.g. Gloeckler and Geiss 1996). They naturally present themselves as candidates for such a population, especially since they have a velocity distribution ranging between zero and roughly twice the solar wind speed (e.g. Vasyliunas and Siscoe, 1976), i.e. exactly where the Monte Carlo model underpredicts the accelerated population for the 91147 event. This population is particularly interesting since the acceleration efficiency of suprathermal ions exceeds that of the thermal particles. The density of pick-up ions in the heliosphere is not uniform due to the gravitational focusing of the ion streams in the solar neighbourhood; in fact, the degree of focusing differs for protons and  $He^+$  (Vasyliunas and Siscoe, 1976) so that the radial variations of the densities of these pick-up species are not the same. Such density gradients are also influenced by variations in the ionization fractions. Helium atoms, whose ionization potential is high, penetrate as close as 0.5AU, whereas hydrogen gas is highly ionized by the time it is less than a few AU from the sun. Hence the density gradient for  $H^+$  is much greater in the 2AU–5AU range than for singly-ionized helium. Note that while  $He^+$  pick-up ions are much more prevalent than  $He^{2+}$  pick-up ions,  $He^{2+}$  is the dominant charge state of helium in the solar wind plasma.

Fortunately, due to measurements by SWICS, as presented by Gloeckler and Geiss (1996), we have a strong indication of the variations in pick-up ion backgrounds at times when the spectra presented in this study were obtained. They indicate that for  $He^+$ , a slow decline in count rate was observed as Ulysses made its way from 1AU to beyond Jupiter (from 2 counts to 0.8 counts per 12 second instrumental sweep), whereas the flux ratio of  $H^+/He^+$  increased by an order of magnitude between 3AU and 5AU. Consequently, it can be inferred that the proton pick-up density increased dramatically during this period of data collection, and specifically, that an increase of a factor of

$\sim 3-5$  occurred between the 91097 and 91147 events. The pick-up ion count rate in the 91147 shock was actually a significant fraction of the proton count rate at comparable suprathermal energies. This implies that the data/theory comparison presented here can comfortably accommodate the hypothesis that there is a very small contribution of pick-up protons for the 91097 shock observed at  $\sim 2.7$  AU, but that this contribution has risen dramatically by day 147 in 1991, corresponding to  $\sim 3.2$  AU. We therefore contend that pick-up ions play an important role in the acceleration process in the 91147 event, and that our omission of them from the Monte Carlo model is primarily responsible for the poor fit.

## 5.2. $\lambda/r_g$ and Field Turbulence

The question of plausibility of the values for  $\lambda/r_g$  obtained by our fits of the spectral data naturally arises. Precedence for such low  $\lambda/r_g$  exists in the literature. Forman, Jokipii and Owens (1974) determined the ratio  $\kappa_{\perp}/\kappa_{\parallel}$  of components of the diffusion tensor along and orthogonal to the field using quasi-linear diffusion theory applied to measurements of the interplanetary magnetic field power spectrum made by the Mariner 4 spacecraft at locations near earth and also near Mars. They computed a ratio of 0.07, which corresponds to  $\lambda/r_g \sim 4$  using the kinetic theory formula in equation (3). Similar estimates are obtained at much larger solar distances ( $\sim 15-20$  AU) using somewhat different analyses of magnetic field data obtained by Voyager 2, to compute  $\kappa_{\perp}$  (see Valdes-Galicia, Quenby and Moussas 1992), and also field data acquired by Pioneer 11 to determine  $\kappa_{\parallel}$  (see Moussas et al. 1992). While these results were obtained using measurements made near the ecliptic plane, it is anticipated that similar estimates will result near the heliospheric poles from information recently acquired by the Ulysses mission. The values for  $\lambda/r_g$  determined from the spectral comparisons here are therefore not extraordinary by heliospheric standards. Yet the diffusion coefficients computed by the analyses of Forman, Jokipii and Owens (1974), Valdes-Galicia, Quenby and Moussas (1992), and Moussas et al. (1992) are all in the range of about  $3 \times 10^{20} \text{ cm}^2 \text{ sec}^{-1} - 3 \times 10^{22} \text{ cm}^2 \text{ sec}^{-1}$ , implying a mean free path of around 1–100 AU for particles of speeds  $v \sim 1000 \text{ km/sec}$  ( $\lambda \sim 3\kappa/v$ ). These far exceed the estimate of a few times  $10^4 \text{ km}$  ( $\sim 3 \times 10^{-4} \text{ AU}$ ) obtainable from equation (4) for similar  $v$  for the IP shocks of studied here. This dramatic difference is very probably not a conflict, but rather reflects a huge disparity in spatial scale of diffusion in the general interplanetary medium as opposed to diffusion in the environs of interplanetary shocks. It must be emphasized that the spectral estimates of  $\lambda/r_g$  determined here are very sensitive to the shock obliquity  $\Theta_{Bn1}$ , a quantity that is difficult to measure accurately in space plasma shocks.

The diffusion length scale associated with interplanetary shocks can be examined by consideration of the magnetic field turbulence in their environs. Fig. 6 displays the magnetic field data measured by the Ulysses magnetometer in the temporal vicinity of the 91097 IP shock on 1 sec (up to the 5.5 hour mark) and 2 sec (more than 5.5 hours into April 7, 1991) timescales. The orthogonal RTN components  $B_R$ ,  $B_T$ ,  $B_N$ , of magnetic field and the total field strength  $|B|$  comprise the

data streams. Here the  $R$ -direction points radially away from the sun, the  $N$ -axis is perpendicular to the  $R$ -axis and lying in the plane formed by the radial vector to the spacecraft and the solar rotation axis, and the  $T$ -direction completes the orthogonal coordinates such that  $R, T$ , and  $N$  form a right-handed system. In Fig. 6a the field quantities are presented for the period of an hour on either side of the 91097 shock to illustrate properties coupled to the shock on smaller scale lengths. The field turbulence appears much larger on the downstream side of the shock (the right hand side of the plot, at later times), but this is somewhat deceptive since there the field has been enhanced due to the shock compression (see the bottom panel). The level of turbulence relative to the mean ambient field is physically a more meaningful quantity, and will be addressed shortly. Also in Fig. 6a there is evidence of sharp discontinuities in field components downstream. These are not shocks since they are not accompanied by steep density gradients, yet they are representative of spatial/temporal structural features generally seen in the turbulent environs of IP shocks. Field data streams for the other candidate shocks look very similar to Fig. 6. In Fig. 6b the field data are displayed for the 4.5 hour period downstream of the shock during which the spectral data in Fig. 3 were collected, revealing no significantly different behaviour from the downstream section in Fig. 6a.

A more illuminating presentation of the turbulent magnetic field is given in Fig. 6, which exhibits the field *turbulence measure*  $|\delta\mathbf{B}|/|\mathbf{B}|$  derived from the measured data in Fig. 6a. The turbulence measure, which can formally be related to the magnetic Reynolds number  $R_M \sim 2|\delta\mathbf{B}|^2/(\mathcal{M}_A|\mathbf{B}|)^2$  (e.g. see Boyd and Sanderson 1969, p. 126), was obtained by comparing vector components of the field in successive time bins (labelled  $i$  and  $i + 1$ ) according to

$$\mathcal{M}_A \sqrt{\frac{R_M}{2}} \sim \frac{|\delta\mathbf{B}|}{|\mathbf{B}|} = \frac{1}{|\mathbf{B}|} \sqrt{\delta B_R^2 + \delta B_T^2 + \delta B_N^2} = \frac{|\mathbf{B}_{i+1} - \mathbf{B}_i|}{|\mathbf{B}_i|} \quad (5)$$

on 1s, 10s and 100s binning timescales. While the choice of turbulence measure is subjective, this definition is informative, and virtually coincides with definition of the normalized variance that is frequently used in the space plasma literature: see Forsyth et al. (1996) for variances during out-of-the-ecliptic passages of Ulysses, which are generally taken as averages over longer terms rather than successive data bins. The remarkable feature of Fig. 6 is the similarity of the turbulence measure on both sides of the shock: the shock enhances the field and the turbulence by similar factors so that the relative level of turbulence remains more or less the same. It is unclear whether or not such a compressive enhancement is caused by shock-generated turbulence. It should be noted that any differences in turbulence measure between the upstream and downstream regions would argue for different values for  $\lambda/r_g$  either side of the shock. However, for the Monte Carlo technique, the key acceleration properties of spectral shape and injection efficiency depend mostly on the value of  $\lambda/r_g$  in the downstream region, so that only this value need be specified. The similarity of the turbulence measures throughout the shock transition further indicates that the added complication of treating such non-uniformities in  $\lambda/r_g$  is unnecessary.

The turbulence measure averages around 5% on second timescales, which is probably around the border of the quasi-linear regime, and increases to an average of 16% on 100 second timescales,

reflecting a non-uniform power spectrum. This latter level of turbulence is quite substantial and is suggestive that quasi-linear theory may not be applicable on these larger timescales. Note that  $|\delta\mathbf{B}|/|\mathbf{B}| > 1$  at the shock on the 1 and 10 second timescales. The binning is truncated at the onset of data gaps in Fig. 6a. Without a more sophisticated analysis (e.g. see Forman, Jokipii and Owens 1974), it is difficult to conclude whether or not these turbulence measures are closely consistent with the spectrally-determined estimates of  $\lambda/r_g$ . However, it is possible to rule out extremities. The Bohm diffusion limit  $\lambda \sim r_g$  is expected to arise when  $|\delta\mathbf{B}|/|\mathbf{B}| \gtrsim 0.5$ , which is not reached in this data. Yet the levels of turbulence are high enough that the plasma is probably much closer to the Bohm diffusion limit than to a  $\lambda/r_g \sim 30$  state. Since the proton gyroperiod is  $T_g = m_p c / (eB) \approx 10.4/B_{-5}$  sec, then protons behind the shock (where  $B \sim 5 \times 10^{-5}$  Gauss) sample fluctuation timescales of the order of a few seconds. This provides a rough guide to the level of turbulence expected to dominate the particle diffusion.

### 5.3. Fermi Acceleration

Another consistency check concerns the acceleration timescale: are the IP shocks old enough to permit the diffusive Fermi mechanism to accelerate ions to the energies observed? Numerous theoretical treatments of diffusive acceleration timescales exist in the literature, and we refer the reader to Jones and Ellison (1991) for a review. For the Monte Carlo technique used here, where the mean free path is proportional to the ion rigidity, an explicit form for the acceleration time to a given energy  $E$  is presented in equation (4) of Ellison, Baring and Jones (1995), and order of magnitude estimates can be gleaned from Fig. 3 of that work. Specifically, the acceleration time  $\tau_a$  is approximately proportional to  $E$ , and yields values of the order of minutes for energization to 10 keV, the typical upper range of SWICS observations, and timescales of the order of a few hours for the MeV energies detected by HI-SCALE. Both these timescales are considerably shorter than the multi-day duration of passage of our candidate IP shocks through the heliosphere, thereby causing no temporal consistency problems for the Fermi mechanism.

It is instructive to remark upon the upstream IP spectral structure and the simulation predictions. The SWICS data upstream of the three candidate shocks are dominated by the beam-like distribution of the solar wind that is thermally-broadened, containing minimal evidence of suprathermal ions. Hence, the measured Upstream densities of  $n_{H^+}$  and  $n_{He^{2+}}$  (for event 91097) are representative of the solar wind properties, containing virtually no pollution from non-thermal ions. Yet, there is marginal evidence in the SWICS data for particles seen upstream at low flux levels but with speeds considerably in excess of the solar wind speed. No continuity of the distribution function is apparent, and it could even be described as consisting of two components of disparate velocities. The upstream non-thermal “component” appears only near the shock. Evidence for such a non-thermal population that wanes with distance from the shock has been seen upstream of interplanetary shocks by previous instruments. Gosling et al. (1984) display distributions that diminish in intensity upstream of IP shocks encountered by ISEE 1 and 2, and that exhibit upstream

non-thermal distributions that are flatter than their downstream counterparts. Tan et al. (1989) present ISEE 3 proton data that impressively exhibits a non-thermal distribution that flattens at greater distances upstream of an IP shock passage.

Such properties are consistent with the theory of Fermi acceleration. Lee’s (1982) analytic modelling of ion acceleration and wave excitation at the Earth’s bow shock predicts that low energy suprathermal ions disappear at short distances upstream of the shock, with a depletion between the solar wind and high speed particles that grows both in size and range of energy as the distance upstream increases. Our Monte Carlo model displays virtually identical properties (Baring, Ellison and Jones 1994; Ellison, Baring and Jones 1996), which are a direct consequence of low energy suprathermal particles having shorter mean paths than ions of higher energies, and therefore having greater difficulty diffusing against the convective power of the solar wind to a given distance upstream of the shock. The ISEE data add weight to the hypothesis that Fermi acceleration is acting at interplanetary shocks.

## 6. CONCLUSION

The spectral comparison between SWICS measurements of ion distributions downstream of three interplanetary shocks observed at 2.7–3.2AU from the sun, and our kinematic Monte Carlo model for diffusive shock acceleration, provides impressive fits of the data for two events (detected on days 91097 and 91118) with theory by effectively varying just a single parameter,  $\lambda/r_g$ . The low values ( $\lesssim 5$ ) of this parameter indicate strong cross-field diffusion (not far from the Bohm diffusion limit) is operating in these systems, a property that is commensurate with magnetic field turbulence in the general interplanetary medium, and is consistent with self-generated turbulence predicted in diverse shock models. Furthermore, the turbulent magnetic field data presented for the 91097 shock appears, without sophisticated analysis, to be concordant with low values of  $\lambda/r_g$  deduced from the spectral considerations. It is anticipated that the inference of strong diffusion normal to the mean ambient magnetic field direction applies to many of the IP shocks encountered by Ulysses during the first half of 1991, since they exhibit similar evidence of prominent downstream non-thermal ion populations.

The Monte Carlo model simulates these complex shock systems in an elegantly simple but elucidating manner, using the measured upstream solar wind quantities as input for the theoretical simulation. It successfully models proton and  $\text{He}^{2+}$  distributions in the 91097 event, both in spectral shape and normalization, using the *same* value of  $\lambda/r_g$ . This is because the acceleration process at IP shocks seems dependent only on the velocity of the species, not its mass or charge. Such a kinematic property is not expected if reflection at the shock layer is an important part of the injection process (e.g. at the quasi-perpendicular portion of the Earth’s bow shock). However, it is an inherent assumption of the Monte Carlo technique in the test-particle acceleration regime that is appropriate for the generally weak IP shocks. The theory makes clear, concise and eminently testable predictions about the fall-off of the accelerated population upstream of shocks; evidence

for this phenomenon occurring at interplanetary shocks already exists in the literature. In the case of the May 27, 1991 shock, the model underpredicts the proton data in the 500–1000km/sec range. We propose that this discrepancy might be rectified if interstellar pick-up protons, which were observed at significant levels during late May 1991 and at subsequent stages of the Ulysses mission, are included in the simulation as an extra population seeding the acceleration process. Anticipated developments of the present work include extension of the comparison to other shocks, and analysis of the field data for the three shocks considered here, using quasi-linear theory, to obtain alternative estimates for the ratio  $\lambda/r_g$ .

We thank Drs. Tom Jones and Len Burlaga for helpful comments following careful reading of the manuscript. We are especially grateful Dr. George Gloeckler, Prof. Johannes Geiss, and the many individuals at the University of Maryland, the University of Bern, the Technische Universität Braunschweig, the Max-Planck-Institut für Aeronomie, and Goddard Space Flight Center who have contributed to the SWICS experiment. We have benefited from discussions with Dr. Daniel Berdichevsky of Hughes/STX, who has been responsible for production of the data. We also thank Dr. Frank Jones, whose encouragement led to our theory/experiment collaboration and the instigation of this project. This work was supported by NASA/JPL contract 955460, the Swiss NSF, the Bundesminister für Forschung and Technologie of Germany, and the NASA Space Physics Theory Program. DCE thanks the Service d’Astrophysique, CEN-Saclay, Observatoire de Paris–Meudon, and CNET/CETP (Issy-les-Moulineaux) for hospitality during much of the period in which work for this paper was completed.

## REFERENCES

- Axford, W. I. 1965, *Planet. Space Sci.* 13, 115.
- Balogh, A., Forsyth, R. J., Ahuja, A., Southwood, D. J., Smith, E. J., and Tsurutani, B. T. 1993, *Adv. Space Sci.* 13, (6) 15.
- Balogh, A., Gonzalez-Esparza, J. A., Forsyth, R. J., Burton, M. E., Goldstein, B. E., Smith, E. J., and Bame, S. J. 1995, *Space Sci. Rev.* 72, 171.
- Baring, M. G., Ellison, D. C. and Jones, F. C. 1993, *ApJ* 409, 327.
- Baring, M. G., Ellison, D. C. and Jones, F. C. 1994, *ApJS* 90, 547.
- Baring, M. G., Ellison, D. C. and Jones, F. C. 1995, *Adv. Space Sci.* 15 (8/9), 397.
- Baring, M. G., Ogilvie, K. and Ellison, D. C. 1995, *Proc. 24th International Cosmic Ray Conference, (Rome)* 3, 229.
- Baring, M. G., Ogilvie, K., Ellison, D. C., and Forsyth, R. 1995, *Adv. Space Sci.* 15 (8/9), 388.
- Bell, A. R. 1978, *MNRAS* 182, 147.
- Blandford, R. D. and Eichler, D. 1987, *Phys. Rep.* 154, 1.
- Boyd, T. J. M. and Sanderson, J. J. 1969, *Plasma Dynamics*, (Barnes and Noble, New York).
- Burton, M. E., Smith, E. J., Goldstein, B. E., Balogh, A., Forsyth, R. J., and Bame, S. J. 1992, *Geophys. Res. Lett.* 19, 1287.
- Decker, R. B. 1988, *Space Sci. Rev.* 48, 195.
- Decker, R. B., Pesses, M. E., and Krimigis, S. M. 1981, *J. Geophys. Res.* 86, 8819.
- de Hoffmann, F. and Teller, E. 1950, *Phys. Rev.* 80, 692.
- Eichler, D.: 1984 *ApJ* 277, 429.
- Ellison, D. C. 1983, in *Proc. 18th International Cosmic Ray Conference, (Bangalore)* 10, 108.
- Ellison, D. C., Baring, M. G. and Jones, F. C. 1995, *ApJ* 453, 873.
- Ellison, D. C., Baring, M. G. and Jones, F. C. 1996, *ApJ*, in press.
- Ellison, D. C. and Eichler, D. 1984, *ApJ* 286, 691.
- Ellison, D. C., Giacalone, J., Burgess, D., and Schwartz, S. J. 1993, *J. Geophys. Res.* 98, 21,085.
- Ellison, D. C., Jones, F. C., and Eichler, D. 1981, *J. Geophys.* 50, 110.
- Ellison, D. C., and Möbius, E. 1987, *ApJ* 318, 474.
- Ellison, D. C., Möbius, E., and Paschmann, G. 1990, *ApJ* 352, 376.
- Forman, M. A., Jokipii, J. R. and Owens, A. J. 1974, *ApJ* 192, 535.
- Forsyth, R. J., Horbury, T. S., Balogh, A. and Smith, E. J. 1996, *Geophys. Res. Lett.* 23, 595.
- Fuselier, S. A., and Schmidt, W. K. H. 1994, *J. Geophys. Res.* 99, 11,539.

- Fuselier, S. A., and Thomsen, M. F. 1992, *Geophys. Res. Lett.* 19, 437.
- Giacalone, J., Burgess, D. and Schwartz, S. J. 1992, in *Proc. 26th ESLAB Symposium, Study of the Solar-Terrestrial System (ESA, Noordwijk)* p. 65
- Giacalone, J., Burgess, D., Schwartz, S. J. and Ellison, D. C. 1992, *Geophys. Res. Lett.* 19, 433.
- Giacalone, J., Burgess, D., Schwartz, S. J. and Ellison, D. C. 1993, *ApJ* 402, 550.
- Gliem, F., et al. 1988, *Solar Wind Ion Composition Spectrometer Data Processing Unit*, technical report of the Technische Universität Braunschweig, Institut für Datenverarbeitungsanlagen.
- Gloeckler, G., et al. 1992, *A&AS* 92, 267.
- Gloeckler, G., and Geiss, J. 1996, in *Cosmic Winds and the Heliosphere*, eds. J. R. Jokipii, et al. (Univ. Arizona Press, Tucson), in press.
- Gloeckler, G., Geiss, J., Roelof, E. C., Fisk, L. A., Ipavich, F. M., Ogilvie, K. W., Lanzerotti, L. J., von Steiger, R., and Wilken, B. 1994, *J. Geophys. Res.* 99, 17,637.
- Gloeckler, G., Roelof, E. C., Ogilvie, K. W., Berdichevsky, D. B. 1995, *Space Sci. Rev.* 72, 321.
- Gosling, J. T., Ashbridge, J. R., Bame, S. J., Feldman, W. C., Zwickl, R. D., Paschmann, G., Scopke, N., and Hynds, R. J. 1981, *J. Geophys. Res.* 86, 547.
- Gosling, J. T., Bame, S. J., Feldman, W. C., Paschmann, G., Scopke, N., and Russell, C. T. 1984, *J. Geophys. Res.* 89, 5409.
- Gosling, J. T., Thomsen, M. F., Bame, S. J., and Russell, C. T. 1989, *J. Geophys. Res.* 94, 3555.
- Gosling, J. T., Bame, S. J., McComas, D. J., Phillips, J. L., Pizzo, V. J., Goldstein, B. E., and Neugebauer, M. 1993, *Geophys. Res. Lett.* 20, 2789.
- Gosling, J. T., Bame, S. J., McComas, D. J., Phillips, J. L., Pizzo, V. J., Goldstein, B. E., and Neugebauer, M. 1995, *Space Sci. Rev.* 72, 99.
- Hoang, S., Lacombe, C., Mangeney, A., Pantellini, F., Balogh, A., Bame, S. J., Forsyth, R. J. and Phillips, J. L. 1995, *Adv. Space Sci.* 15 (8/9), 371.
- Hoppe, M. M., Russell, C. T., Frank, L. A., Eastman, T. E., and Greenstadt, E. W. 1981, *J. Geophys. Res.* 86, 4471.
- Hundhausen, A. J. 1973, *J. Geophys. Res.* 78, 1528.
- Ipavich, F. M., Scholer, M. and Gloeckler, G. 1981, *J. Geophys. Res.* 86, 11,153.
- Ipavich, F. M., Gloeckler, G., Hamilton, D. C., Kistler, L. M., and Gosling, J.T. 1988, *Geophys. Res. Lett.* 15, 1153.
- Jokipii, J. R. 1987, *ApJ* 313, 842.
- Jokipii, J. R., and Jones, F. C. 1996, *Phys. Rev. Lett.*, submitted.
- Jokipii, J. R., Kóta, J., and Giacalone, J. 1993, *Geophys. Res. Lett.* 20, 1759.
- Jones, F. C. and Ellison, D. C. 1991, *Space Sci. Rev.* 58, 259.

- Jones, T. W. and Kang, H. 1995, Proc. 24th International Cosmic Ray Conference, (Rome) 3, 245.
- Kang, H. and Jones, T. W. 1995, ApJ 447, 944.
- Kang, H. and Jones, T. W. 1996, ApJ in press.
- Kennel, C. F., et al. 1984, J. Geophys. Res. 89, 5436.
- Kucharek, H. and Scholer, M. 1995, J. Geophys. Res. 100, 1745.
- Lanzerotti, L. J., Gold, R. E., Anderson, K. A., Armstrong, T. P., Lin, R. P., Krimigis, S. M., Pick, M., Roelof, E. C., Sarris, E. T., Simnett, G. M., and Frain, W. E. 1992, A&AS 92, 349.
- Lee, M. A. 1982, J. Geophys. Res. 87, 5063.
- Liewer, P. C., Goldstein, B. E., and Omid, N. 1993, J. Geophys. Res. 98, 15,211.
- Liewer, P. C., Rath, S., and Goldstein, B. E. 1995, J. Geophys. Res. 100, 19,809.
- Mason, G. M., Gloeckler, G., and Hovestadt, D. 1983, ApJ 267, 844.
- Möbius, E., Scholer, M., Skopke, N., Lühr, H., Paschmann, G., and Hovestadt, D. 1987, Geophys. Res. Lett. 14, 681.
- Moussas, X., Quenby, J. J., Theodossiou-Ekaterinidi, Z., Valdes-Galicia, J. F., Drillia, A. G., Roulias, D. and Smith, E. J. 1992, Sol. Phys. 140, 161.
- Ogilvie, K. W., Geiss, J., Gloeckler, G., Berdichevsky, D. B., and Wilken, B. 1993, J. Geophys. Res. 98, 3605.
- Phillips, J. L., Bame, S. J., Gary, S. P., Gosling, J. T., Scime, E. E. and Forsyth, R. J. 1995, Space Sci. Rev. 72, 109.
- Sarris, E. T., and Van Allen, J. A. 1974, J. Geophys. Res. 79, 4157.
- Scholer, M., Ipavich, F. M., Gloeckler, G., and Hovestadt, D. 1980, J. Geophys. Res. 85, 4602.
- Tan, L. C., Mason, G. M., Gloeckler, G., and Ipavich, F. M. 1988, J. Geophys. Res. 93, 7225.
- Tan, L. C., Mason, G. M., Gloeckler, G., and Ipavich, F. M. 1989, J. Geophys. Res. 94, 6552.
- Thomsen, M. F. 1985, in Collisionless Shocks in the Heliosphere: Reviews of Current Research, Geophys. Monogr. Ser., 35, eds. B.T. Tsurutani and R.G. Stone (AGU, Washington, DC), p. 253.
- Trattner, K. J., and Scholer, M. 1991, Geophys. Res. Lett. 18, 1817.
- Trattner, K. J., and Scholer, M. 1993, Ann. Geophysicae 11, 774.
- Tsurutani, B. T., Smith, E. J., and Jones, D. E. 1983, J. Geophys. Res. 88, 5645.
- Valdes-Galicia, J. F., Quenby, J. J., and Moussas, X. 1992, Sol. Phys. 139, 189.
- Vasyliunas, V. M., and Siscoe, G. L. 1976, J. Geophys. Res. 81, 1247.
- Viñas, A. F., Goldstein, M. L., and Acuña, M. H. 1984, J. Geophys. Res. 89, 3762.

TABLE 1

OBSERVED SOLAR WIND QUANTITIES: INPUT FOR MONTE CARLO SIMULATIONS

	April 7, 1991 2.7 AU (91097)	April 28, 1991 2.85 AU (91118)	May 27, 1991 3.15 AU (91147)	Notes
$u_s$ [km s <sup>-1</sup> ]	153	165	132	(1)
$\Theta_{Bn1}$	77° ± 7°	75° ± 7°	55° ± 16°	(2)
$v_{th}(H^+)$ [km s <sup>-1</sup> ]	23 ± 2	29 ± 3	50 ± 2	(3)
$v_{th}(He^{2+})$ [km s <sup>-1</sup> ]	26 ± 3	...	...	(3, 4)
$n_{H^+}$ [cm <sup>-3</sup> ]	1.4 ± 0.1	0.37 ± 0.03	3.0 ± 0.3	
$n_{He^{2+}}$ [cm <sup>-3</sup> ]	0.06 ± 0.005	...	...	(4)
$B_1$ [10 <sup>-5</sup> Gauss]	2.05 ± 0.05	1.95 ± 0.05	4.30 ± 0.05	(5)
$T_e$ [10 <sup>4</sup> K]	6.4	6.5	12.4	(6)
$T_{H^+}$ [K]	3.2 × 10 <sup>4</sup>	4.9 × 10 <sup>4</sup>	1.5 × 10 <sup>5</sup>	(7)
$T_{He^{2+}}$ [K]	1.6 × 10 <sup>5</sup>	...	...	(4, 7)
$\mathcal{M}_S$	4.21	4.17	2.15	(8)
$\mathcal{M}_A$	4.05	2.39	2.44	
$\mathcal{M}_T$	2.92	2.07	1.61	(9)

Notes: (1) Shock velocities (relative to solar wind) for 91097 and 91147 were taken from Burton et al. (1992), but that for 91118 was estimated from the value of  $\mathcal{M}_S$  inferred from the  $\mathcal{M}_T$  given by Burton et al. (2) Shock obliquities were taken from Burton et al. (1992) and their uncertainties are given in Balogh et al. (1995). (3) The thermal velocities  $v_{th}$  are measured Gaussian widths. (4) Omissions in  $He^{2+}$  data occur where such information was not used in the present comparison. (5) Mean upstream fields  $B_1$  are taken from magnetometer measurements (Hoang et al. 1995). (6) Electron temperatures for 91097 and 91147 are from (Hoang et al. 1995), while that for 91118 was estimated using the large scale averages of Phillips et al. (1995). (7) Ion temperatures are from  $T_i = m_i v_{th}^2 / (2k)$ . (8) The  $\mathcal{M}_S$  values assume that  $n_e = n_{H^+}$ , and have included the dynamical effects of  $He^{2+}$ . (9) Here  $\mathcal{M}_T = \mathcal{M}_S \mathcal{M}_A / \sqrt{\mathcal{M}_S^2 + \mathcal{M}_A^2}$ . Uncertainties are quoted for measured quantities. See the text for further elaboration on these parameters.

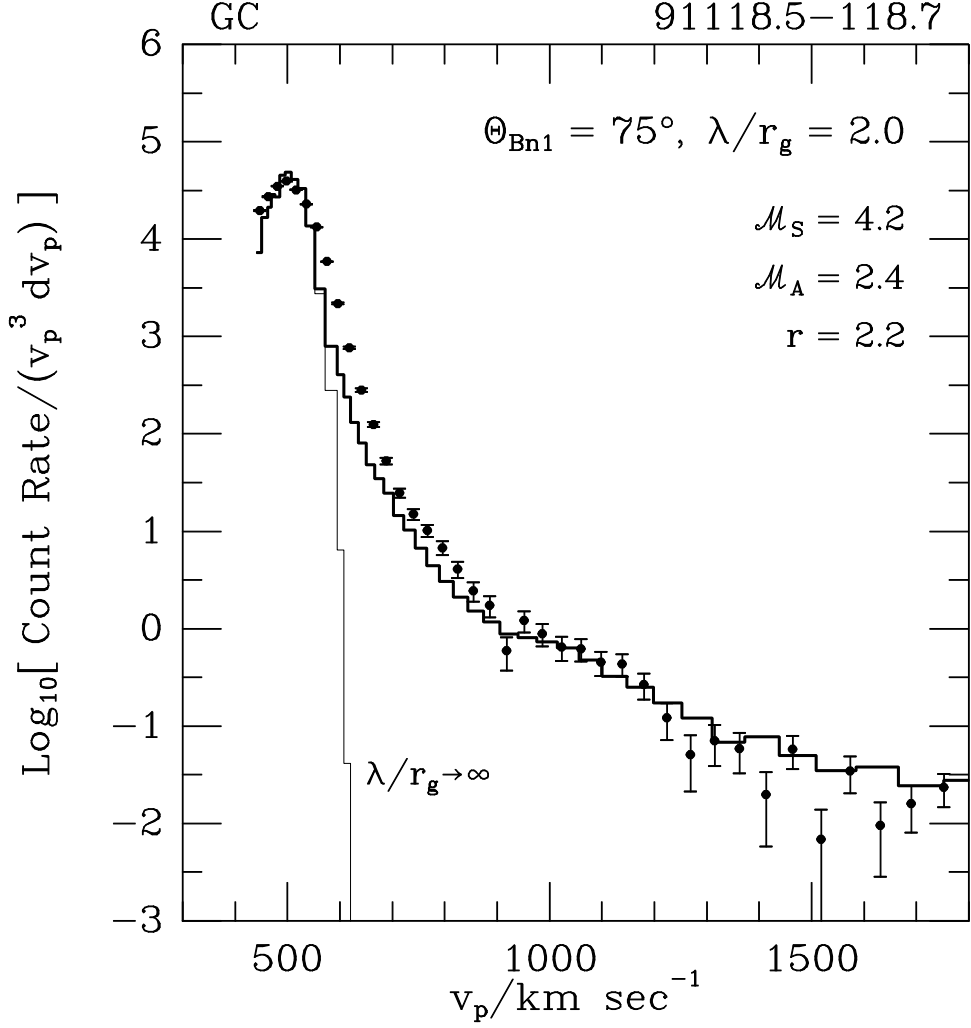


Fig. 1.— Comparison of the SWICS  $H^+$  data (points define the phase-space distribution, measured in the spacecraft frame and certain at the  $1\sigma$  level) for the quasi-perpendicular interplanetary shock on April 28, 1991 (91118), taken over a period of a few hours on the downstream side where the distribution was relatively steady in time, and the Monte Carlo simulation output spectrum (histogram) from the guiding-center (GC) implementation of the code. The mean measured shock obliquity of  $75^\circ$  and other observed shock parameters (see Table 1) were used to yield model parameters such as the compression ratio,  $r$ , and the sonic  $\mathcal{M}_S$  and Alfvénic  $\mathcal{M}_A$  Mach numbers, as indicated. The value of  $\lambda_0/r_{g1}$  ( $=\lambda/r_g$ ), adjusted to obtain the fit, indicates that moderately strong scattering is operating in this shock. The light solid histogram is the simulated distribution in the limit of  $\lambda/r_g \rightarrow \infty$ . The count rate axis is expressed in units of  $\text{km}^{-7} \text{sec}^4$ . For reference, proton speeds of 1000 km/sec correspond to a kinetic energy of 5.22 keV.

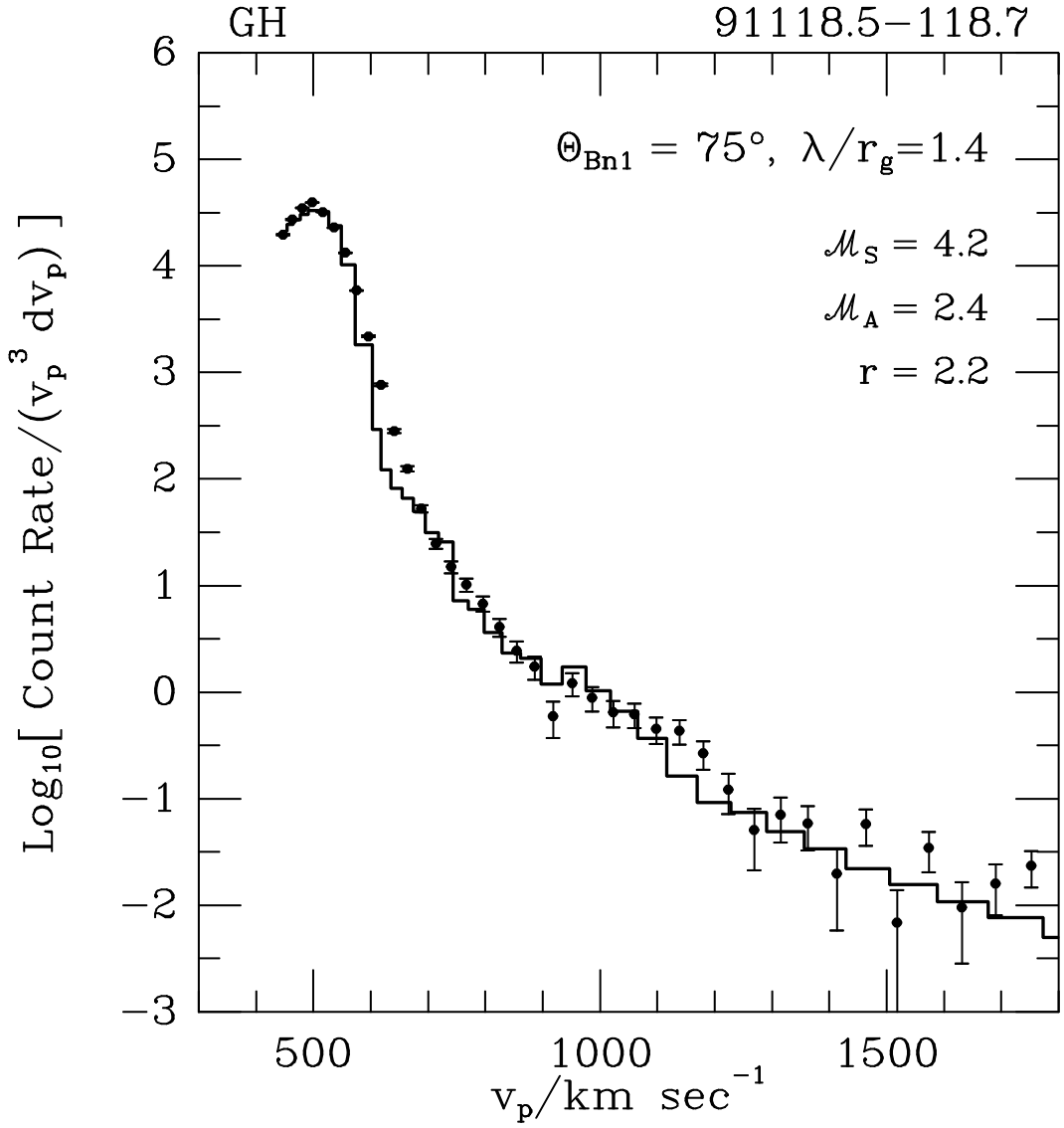


Fig. 2.— The same SWICS proton data as in Fig. 1 are presented, but here are compared with an output spectrum from the version of the Monte Carlo code that computes particle gyrohelices (GH) exactly. The similarity of the values of  $\lambda/r_g$  in Fig. 1 and obtained here that are required to fit the data indicate that the Monte Carlo model is largely insensitive to the details of particle gyromotions. These extremely low values of  $\lambda/r_g$  are a direct consequence of the weakness of the shock (i.e low  $r$ ).

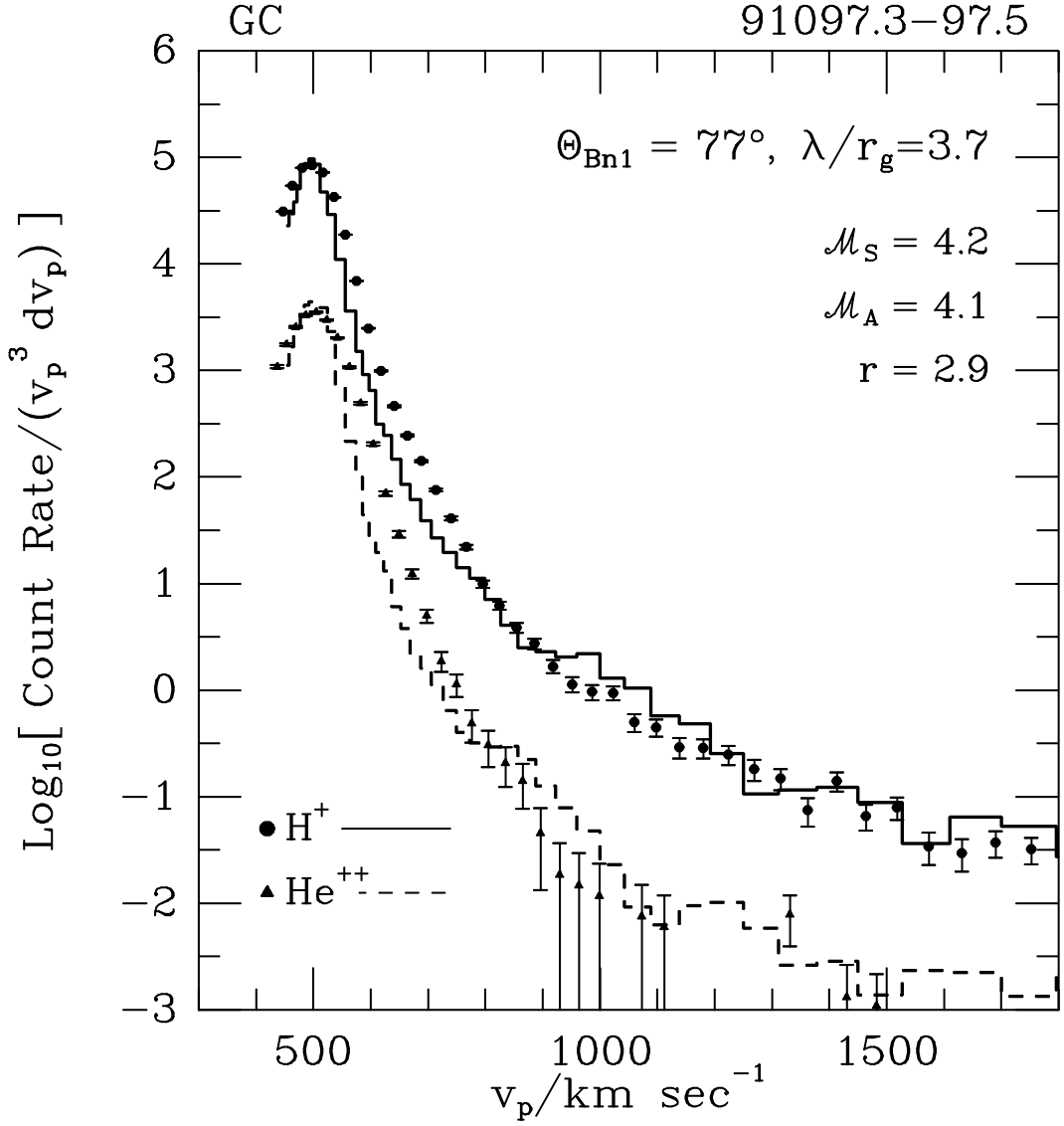


Fig. 3.— Phase-space distributions for ionized hydrogen (filled circles) and alpha particles (filled triangles), measured downstream of the April 7, 1991 (91097) shock by SWICS, again over a period of several hours. The solid and dashed histograms are the Monte Carlo simulation (guiding-center version, GC) predictions for  $H^+$  and  $He^{2+}$ , respectively, and the impressive fit implies the presence of very strong scattering, a species-independent acceleration process (see text for discussion), and also the absence of pick-up ions in this shock. The higher compression ratio of this shock compared with 91118 resulted in a higher fitting value of  $\lambda/r_g$ .

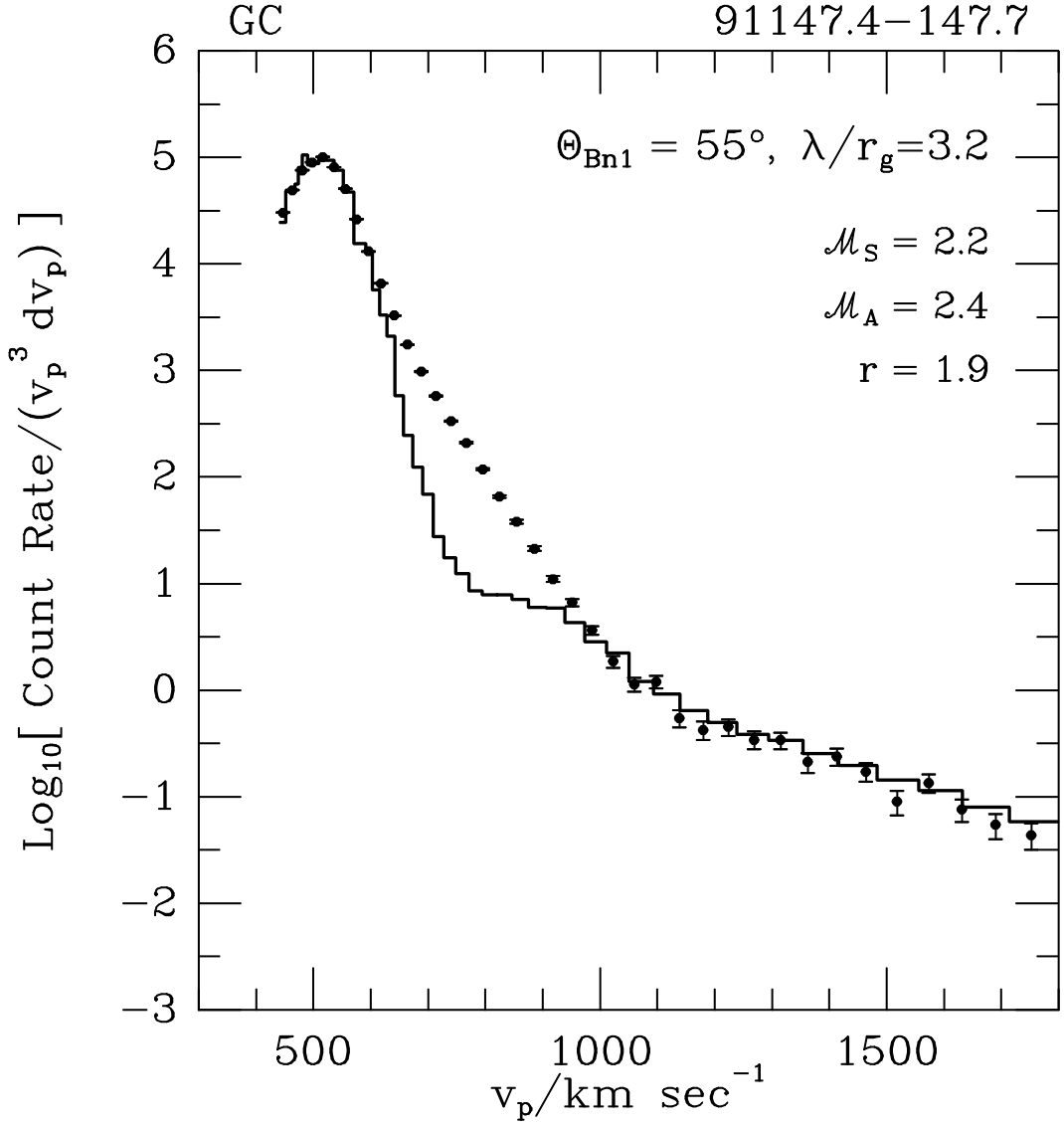


Fig. 4.— A similar comparison to that in Figs. 1 and 3, but for the oblique interplanetary shock detected on May 27, 1991 (91147), again taken over a period of a few hours on the downstream side where the distribution was relatively steady in time. The guiding-center version of the Monte Carlo code was again used to obtain the fit. Strong scattering ( $\lambda/r_g \lesssim 10$ ) is indicated. The comparative inaccuracy of the fit in the suprathermal regime suggests the presence of another population of particles: the presence of pick-up ions might be inferred for this shock, which was about 0.45 AU further from the sun (see Table 1) than 91118.

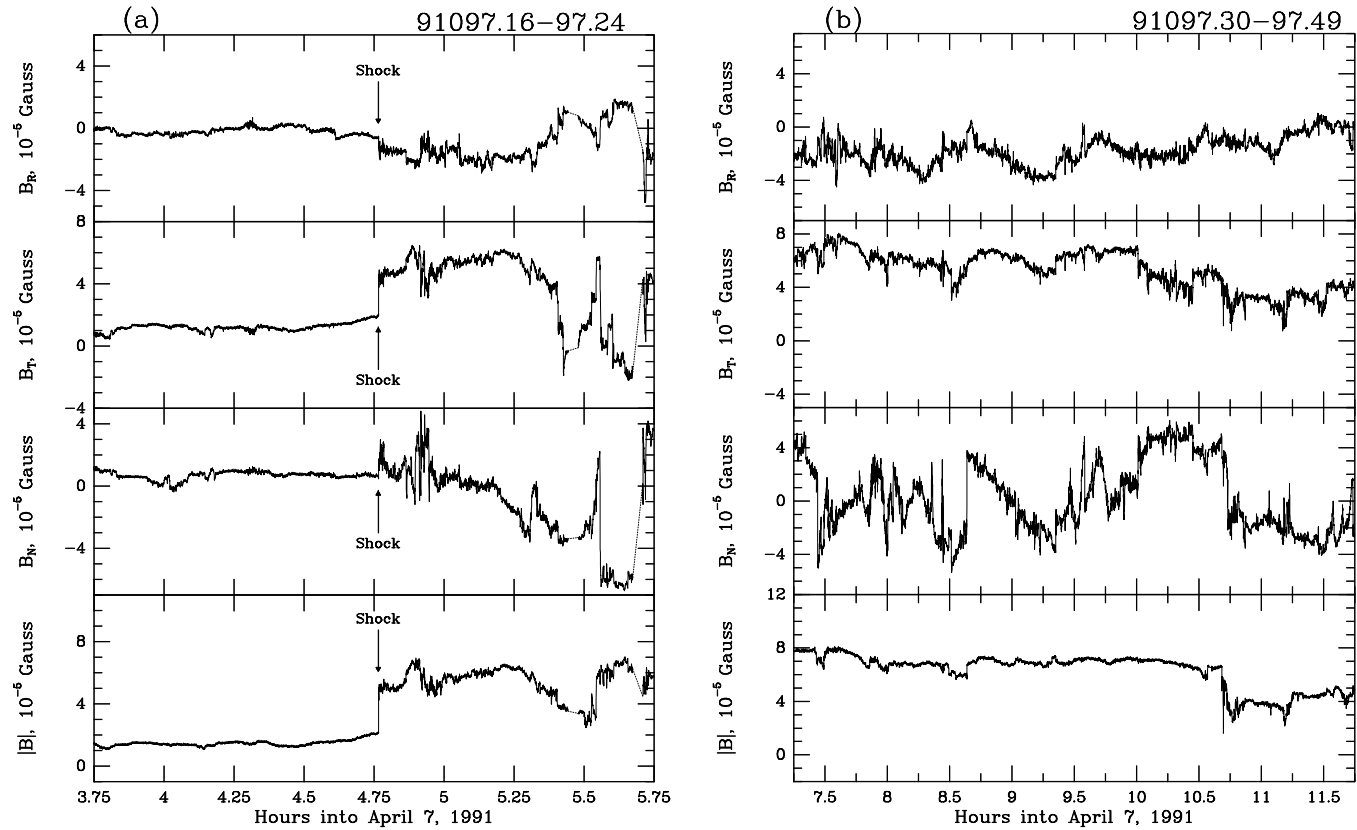


Fig. 5.— The RTN components ( $B_R$ ,  $B_T$ ,  $B_N$ : see text for definition) of magnetic field and the total field strength  $|B|$  measured by the Ulysses magnetometer as a function of spacecraft time, for (a) an hour on either side of the 91097 shock, and (b) for the 4.5 hour period downstream of the shock during which the spectral data in Fig. 3 were collected. Data was binned mostly on 1 second timescales in (a), but at times after hour 5.5, two second bins are presented. The turbulence is considerable everywhere, and is of larger scale downstream of the shock where the total field is larger. Dashed lines in (a) correspond to data gaps.

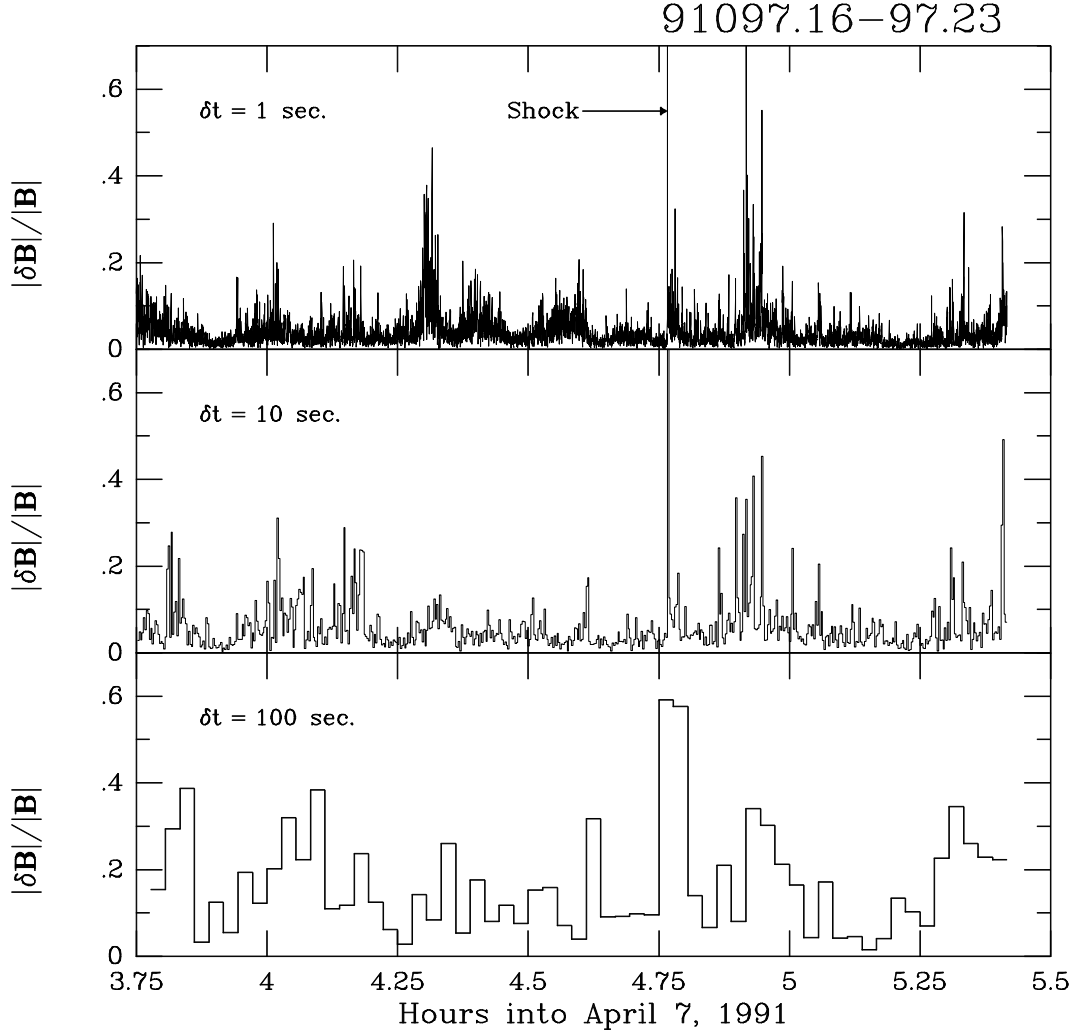


Fig. 6.— The turbulence measure  $|\delta\mathbf{B}|/|\mathbf{B}|$ , defined in Eq. (5), for times surrounding the 91097 shock, obtained using the field data displayed in Fig. 5a. Binning is exhibited on three timescales  $\delta t$ , as labelled, indicating a slow increase in turbulence measure with timescale. Clearly the degree of turbulence is similar either side of the shock, therefore indicating that in Fig. 5,  $|\delta\mathbf{B}|$  scales with  $|\mathbf{B}|$ . The data at the shock for timescales of 1 and 10 seconds yield  $|\delta\mathbf{B}|/|\mathbf{B}|$  in excess of unity.